

# RSC Advances



This is an *Accepted Manuscript*, which has been through the Royal Society of Chemistry peer review process and has been accepted for publication.

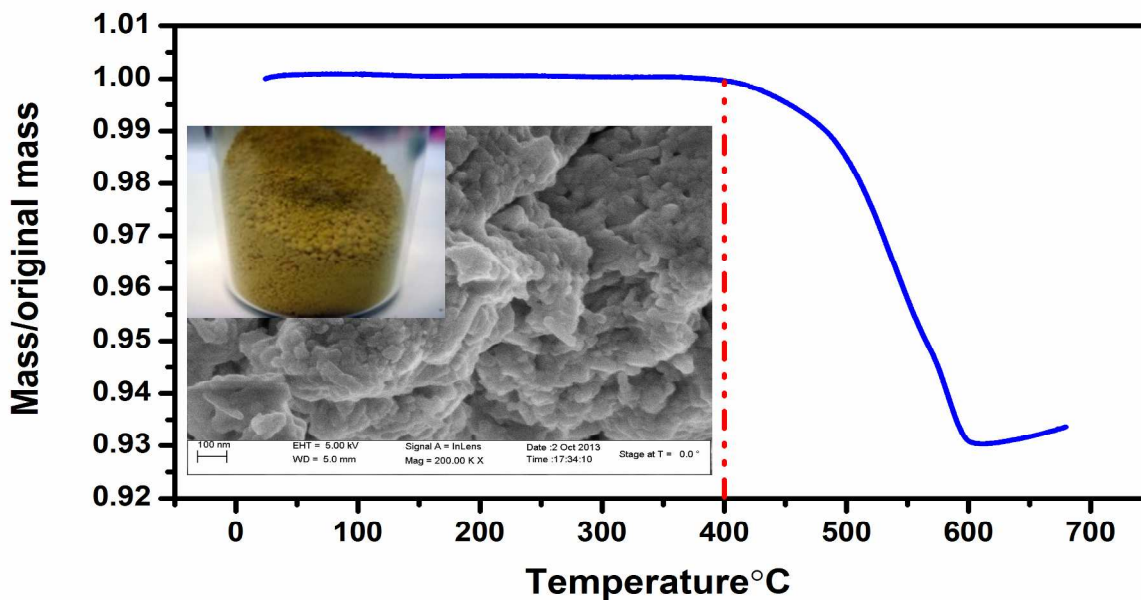
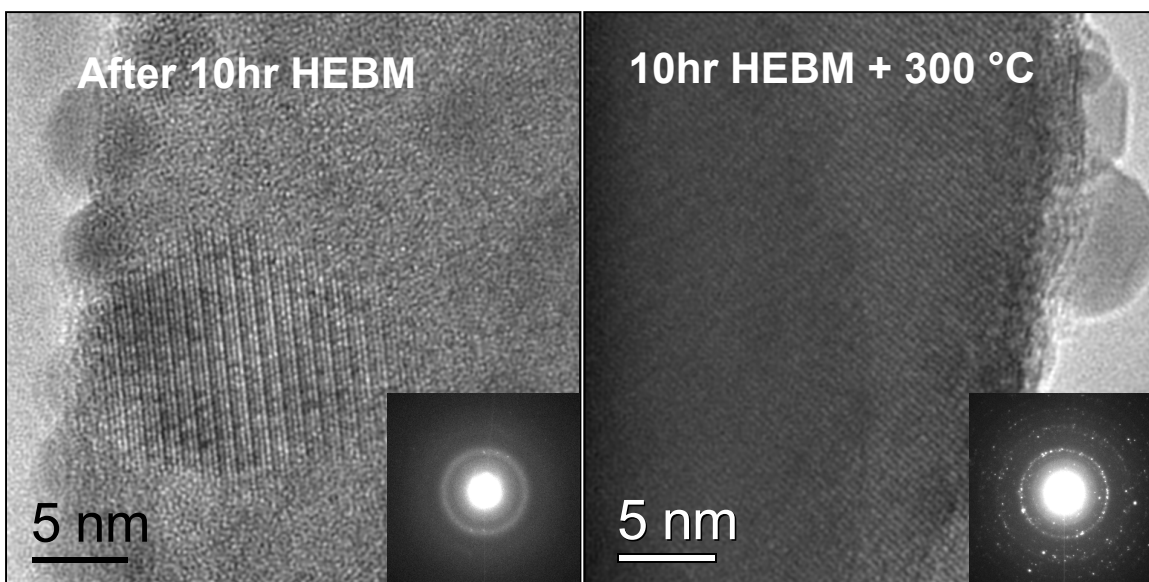
*Accepted Manuscripts* are published online shortly after acceptance, before technical editing, formatting and proof reading. Using this free service, authors can make their results available to the community, in citable form, before we publish the edited article. This *Accepted Manuscript* will be replaced by the edited, formatted and paginated article as soon as this is available.

You can find more information about *Accepted Manuscripts* in the [Information for Authors](#).

Please note that technical editing may introduce minor changes to the text and/or graphics, which may alter content. The journal's standard [Terms & Conditions](#) and the [Ethical guidelines](#) still apply. In no event shall the Royal Society of Chemistry be held responsible for any errors or omissions in this *Accepted Manuscript* or any consequences arising from the use of any information it contains.

## Graphical Abstract

High energy ball milled iodoapatite in the form of amorphous matrix embedded with nanocrystals can be readily crystallized by low temperatures post thermal annealing, which greatly improves the thermal stability and iodine confinement.



Cite this: DOI: 10.1039/c0xx00000x

www.rsc.org/xxxxxx

ARTICLE TYPE

# Facile Low Temperature Solid State Synthesis of Iodoapatite by High-Energy Ball Milling

Fengyuan Lu,<sup>a</sup> Tiankai Yao,<sup>a</sup> Jinling Xu,<sup>a</sup> Jingxian Wang,<sup>b</sup> Spencer Scott,<sup>a</sup> Zhili Dong,<sup>b</sup> Rodney C. Ewing<sup>c</sup> and Jie Lian<sup>\*a</sup>

Received (in XXX, XXX) Xth XXXXXXXXX 20XX, Accepted Xth XXXXXXXXX 20XX  
DOI: 10.1039/b000000x

The apatite structure-type has been proposed as a potential waste form for the immobilization of long-lived fission products, such as I-129; however, it is difficult to synthesize iodoapatite without significant iodine loss due to its high volatility. In this study, we report a facile low temperature (~ 50 °C) solid-state method for successfully synthesizing lead-vanadate iodoapatite by high-energy ball milling (HEBM) of constituent compounds: PbI<sub>2</sub>, PbO and V<sub>2</sub>O<sub>5</sub>. As-milled iodoapatite is in the form of amorphous matrix embedded with nanocrystals and can be readily crystallized by subsequent thermal annealing at a low temperature of 200 °C with minimal iodine loss. Rietveld refinement of the X-ray diffraction patterns indicates that the thermally-annealed iodoapatite is iodine deficient with the iodine concentration of ~4.2 at.%. Thermal gravimetric analysis (TGA) indicates that low temperature annealing greatly improves the thermal stability and iodine confinement. This novel approach, using HEBM and thermal annealing, is a very promising method for synthesizing advanced materials that can confine highly volatile radionuclides, such as I-129, which pose significant challenges for the successful disposal of high-level nuclear waste.

## 1. Introduction

The immobilization and disposal of I-129, a long-lived fission product element ( $t_{1/2} = 15.7$  million years), is critical to the effective management of high-level radioactive waste.<sup>1</sup> I-129 is highly mobile because it forms negatively charged species in solution; thus, it requires a specially-designed, durable waste form for its immobilization. There have been a number of efforts to incorporate I-129 into a durable matrix for deep geological disposal.<sup>1-5</sup> The apatite-type structure  $A^{I}_4A^{II}_6(BO_4)_6X_2$  ( $A^I, A^{II} = Ca, Na, \text{rare earths, fission products such as Sr, and/or actinides; } B = Si, P, V, \text{ or Cr; and } X = OH, F, Cl, \text{ or O}$ ) offers the advantages of high waste loading, high chemical durability and “tunable” radiation stability.<sup>3,6</sup> A wide range of actinides and fission products can be incorporated into apatite structure as a result of its structural flexibility and complex crystal chemistry upon coupled cation and anion substitutions. Particularly, apatite has an open frame structure consisting of six equivalent  $BO_4$  tetrahedra corner-connected to  $AO_6$  metaprisim columns, forming a one-dimensional channel parallel to the *c* axis of the hexagonal structure. Large A-site cations create a larger channel capable of accommodating X-anions, such as iodine. In contrast, smaller A-site cations reduce channel size, which may lead to X anion vacancies and non-stoichiometric apatite compositions.<sup>7,8</sup> Lead vanadate iodoapatite  $Pb_{10}(VO_4)_6I_2$  has large A- and B-site atoms of Pb and V that enable the accommodation of the high concentrations of iodine anions in the tunnel and has thus been proposed as a promising waste form for the immobilization of I-129. The theoretical iodine loading estimated from the

stoichiometric composition is ~8.4 wt.%.

Extensive research has been conducted on the synthesis and testing of  $Pb_{10}(VO_4)_6I_2$  type iodoapatite for iodine confinement and disposition. A previous *ab initio* calculation estimated the standard enthalpy of formation for stoichiometric iodoapatite to be -1298.471 kcal/mol, suggesting that the iodoapatite may be thermodynamically stable at room temperature.<sup>9</sup> Efforts to synthesize iodine-bearing apatite date back to the 1950s,<sup>10</sup> and are currently attracting renewed interests due to the increasing concerns over the waste management of I-129.<sup>3, 11, 12</sup> Conventional hot pressing method has been used to synthesize the lead vanadate iodoapatite at sintering temperatures of approximately 700 °C, and structural analysis by Audubert *et al.*<sup>13</sup> showed an iodine-deficient, Pb-apatite structure-type with a composition of  $Pb_{9.85}(VO_4)_6I_{1.7}$  and a theoretical density of 6.935 g/cm<sup>3</sup>. A significant iodine loss may occur during synthesis process due to the high volatility of iodine and a phase decomposition of lead-vanadate iodoapatite (*e.g.*,  $Pb_{10}(VO_4)_6I_2$  or  $Pb_{9.85}(VO_4)_6I_{1.7}$ ) to orthovanadate  $Pb_3(VO_4)_2$  at ~270 °C and a complete iodine loss occurs at ~400 °C.<sup>14</sup> As a result, highly isolated systems such as sealed containers or encapsulating ceramics are needed for the synthesis of iodoapatite by solid state reaction at elevated temperature in order to prevent potential iodine loss.<sup>1, 3, 15</sup> Recently, novel techniques such as reactive microwave dielectric heating<sup>12</sup> and spark plasma sintering (SPS)<sup>11</sup> have been developed for the synthesis of lead vanadate iodoapatite. Rapid heating of the materials resulting from field assisted sintering helps to prevent significant iodine loss. However, these methods still involve chemical reaction at

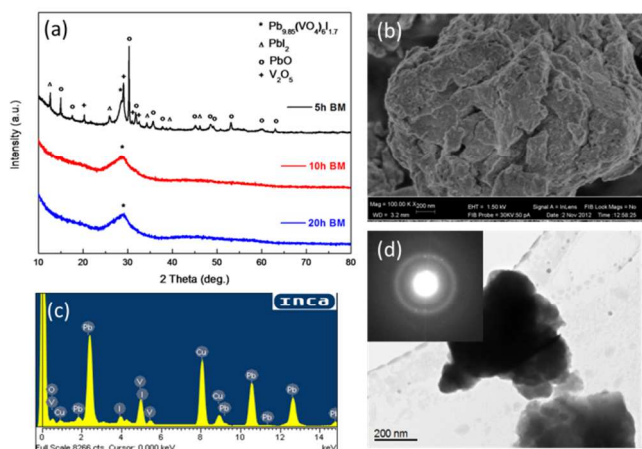


**Fig. 1** (a) XRD patterns of ball-milled powders with different milling times; (b) a SEM image of an as-milled sample (20 hr milling) displaying micron-sized granules consisting of consolidated nano-sized particles; (c) and (d): a EDS spectrum and a bright field TEM image showing the successful fabrication of I-apatite by high-energy ball milling and nano-sized -microstructures in the as-milled sample.

elevated temperatures by heating the samples. As a result, the development of a low temperature solid state approach for synthesizing iodoapatite without release of radioactive iodine is critical for safe immobilization and disposal of problematic I-129. In the present work, we demonstrate a one-step facile route for synthesizing iodoapatite via a low temperature solid-state reaction by a high energy ball mill (HEBM). The solid-state reaction, targeting the  $\text{Pb}_{10}(\text{VO}_4)_6\text{I}_2$ -based iodoapatite structure, was energized solely by mechanical attrition induced by HEBM without any heating, leading to nanocrystals embedded into an amorphous matrix. The ball-milled, amorphous iodoapatite can be crystallized by subsequent thermal annealing at a relatively low temperature of 200 °C. Chemical analysis indicated that no iodine loss occurred upon low temperature thermal annealing, and the iodine waste loading is above 7 wt%, close to the maximum waste loading defined by the structural stoichiometry. The efficient synthesis of iodoapatite by HEBM and subsequent annealing provides a new pathway for the development of advanced iodine bearing waste forms with minimum iodine-loss.

## 2. Experimental Procedure

The HEBM process was carried out in a Fritsch Pulverisette 7 Premium Line planetary ball mill following simple and efficient procedures. Specifically, commercially-available micron-sized  $\text{PbI}_2$  (99.5% purity),  $\text{PbO}$  (99.3% purity) and  $\text{V}_2\text{O}_5$  (99.1% purity) powders were mixed in a molar ratio of 1:9:3 as the starting materials. In a typical run, 10 g of these powders were milled with 5 ml of ethanol by 100 g of 2 mm diameter  $\text{ZrO}_2$  milling balls in an 80 ml  $\text{ZrO}_2$  milling bowl. The mixtures were milled at a speed of 500 rpm at varied durations of 5, 10 and 20 hours, respectively. During the milling process, the temperature and pressure inside the milling bowl were monitored by an Easy GTM sensor. After the milling, the powders were dried and separated from the milling balls, and subsequent thermal annealing was performed on as-milled powders at different temperatures of 200, 300, 400 and 550 °C in air for 1 hour, respectively.

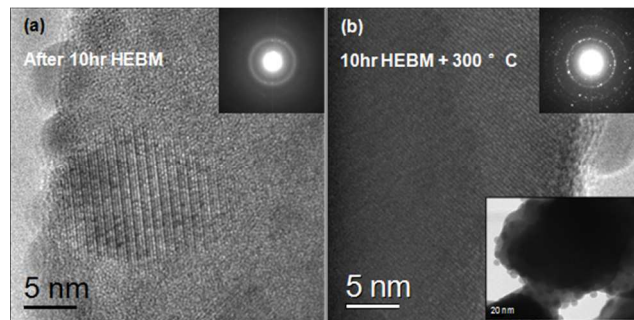


**Fig. 2** (a) HRTEM image and SAED pattern (inset) of the 10 hr-ball milled sample showing iodoapatite nanocrystals embedded in an amorphous matrix; (b) HRTEM image inset with a lower magnification image and SAED pattern of the 300 °C treated sample showing significant crystallization and grain growth.

The morphology, microstructure and chemical composition of as-milled and thermally-treated samples were characterized by a JEOL 2010 transmission electron microscopy (TEM) and by a Zeiss Supra 55 scanning electron microscopy (SEM). Crystal structures were analyzed by X-ray diffraction (XRD) with a PANalytical X'pert Pro X-ray diffractometer, and the Rietveld structural refinement of the XRD data was done with TOPAS software. To determine the phase transition temperature of the as-milled samples, differential scanning calorimetry (DSC) was conducted in a DSC-Q100 instrument (TA instrument, US). The powder samples were loaded into a covered aluminum pan in a nitrogen atmosphere with a nitrogen flow rate of 50 ml/min, followed by a thermal cycle of heating to 510 °C at a heating rate of 5 °C/min and then cooling down to room temperature at 10 °C/min. Thermal gravimetric analysis (TGA) was performed in a TGA-Q50 (TA instrument, US) system to determine the weight loss during heating from room temperature to 510 °C under flowing air at a heating rate of 5 °C/min.

## 3. Results and Discussion

### 3.1 Materials Synthesis by High Energy Ball Milling

Simple binary oxides and iodide of  $\text{PbI}_2$ ,  $\text{PbO}$  and  $\text{V}_2\text{O}_5$  in a molar ratio of 1:9:3 were selected as the starting materials for HEBM synthesis of iodoapatite in order to target the stoichiometric composition of  $\text{Pb}_{10}(\text{VO}_4)_6\text{I}_2$ . Ethanol was used for wet grinding to improve the milling efficiency and prevent agglomeration and chunk formation. During the high energy ball milling, the temperature and pressure inside the bowl slightly increased to ~ 50 °C and ~ 1.5 bars as monitored by the Easy GTM sensor. The high impact velocities and frequencies of the grinding media bring the materials into a highly non-equilibrium state, consequently inducing a solid state chemical reaction among the ingredients:  $\text{PbI}_2 + 9\text{PbO} + 3\text{V}_2\text{O}_5 \rightarrow \text{Pb}_{10}(\text{VO}_4)_6\text{I}_2$ . The XRD data in Fig. 1A indicate that the iodoapatite began to form after 5 hours of milling, and the appearance of a diffraction peak at  $2\theta = 28^\circ$  suggested the formation of intended phase assemblage of iodoapatite. However, due to the short ball milling duration, there are still unreacted  $\text{PbI}_2$ ,  $\text{PbO}$  and  $\text{V}_2\text{O}_5$  traced in the obtained powders. A complete reaction was achieved after 10 hours of milling, as the original binary oxide and iodide peaks fully disappeared and the characteristic iodoapatite (112) peak, centered at  $2\theta$  of ~ 28°, became prominent. An increase in

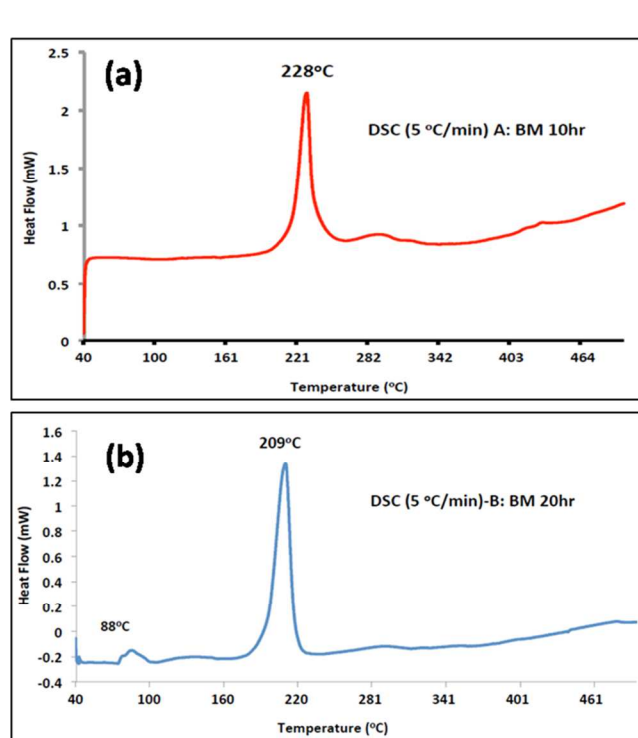
Cite this: DOI: 10.1039/c0xx00000x

www.rsc.org/xxxxxx

## ARTICLE TYPE

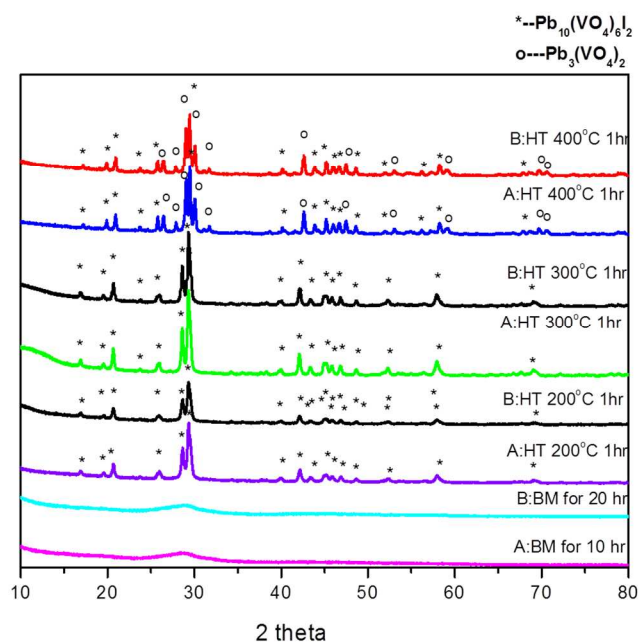
**Table 1** EDS element analysis (at%) of the 10 hr as-milled sample and thermally treated samples (3 columns on the left), as compared to the element compositions for stoichiometric  $\text{Pb}_{10}(\text{VO}_4)_6\text{I}_2$ , non-stoichiometric  $\text{Pb}_{9.85}(\text{VO}_4)_6\text{I}_{1.7}$  and lead vanadate  $\text{Pb}_3(\text{VO}_4)_2$ .

Element at. %	10 h HEBM	10 h HEBM + 200 °C	10 h HEBM + 200 °C	10 h HEBM + 400 °C	Stoichiometric $\text{Pb}_{10}(\text{VO}_4)_6\text{I}_2$	$\text{Pb}_{9.85}(\text{VO}_4)_6\text{I}_{1.7}$	$\text{Pb}_3(\text{VO}_4)_2$
V	12.00	12.54	12.27	11.78	14.28	14.44	15.38
I	4.18	4.14	3.58	1.12	4.76	4.09	0
Pb	26.91	25.98	26.73	28.83	23.81	23.71	23.08
O	56.91	57.34	57.42	58.27	57.15	57.76	61.54

**Fig. 3** DSC curves of the as-milled iodoapatite samples: (a) 10 h milled and (b) 20 h milled with a heating rate of 5 °C/min.

milling time to 20 hours has no significant effects on the phase assemblage and structure. Significant peak broadening and overlapping of the iodoapatite (121), (112) and (300) diffractions centered at  $2\theta$  of  $\sim 28^\circ$  were observed in both 10 h and 20h milled samples, implying the formation of nanostructure. Fig. 1B is a SEM image of the as-milled sample (after 20 hrs milling) showing the morphology of micron-sized granular consisting of consolidated nanoparticles for the I-apatite, and the morphology is typically observed for the materials prepared by high energy ball milling.

Energy-dispersive X-ray spectroscopy (EDS) measurements of the as-milled samples were performed using TEM (as shown in Fig. 1C). Signal of iodine can be clearly seen in the EDS spectrum, indicating the confinement of iodine upon the formation of the single-phase apatite after high energy ball milling. Quantification analysis of EDS data (see Table 1)

**Fig. 4** XRD patterns of thermally treated samples at 200 °C, 300 °C and 400 °C for 1 hour for both 10 h and 20 h milled samples. Amorphous-dominant iodoapatite began to form after 10 h and 20 h ball milling. A pure and highly crystalline iodoapatite was obtained by 200 °C and 300 °C thermal treatments; and a further increase in temperature to 400 °C led to the formation of  $\text{Pb}_3(\text{VO}_4)_2$  as a result of iodoapatite phase decomposition and iodine loss.

indicates that the 10 h milled sample is an iodine-bearing phase with  $\sim 4.2$  at% iodine content. The waste loading of iodine is close to the atomic percentage in the previously-reported  $\text{Pb}_{9.85}(\text{VO}_4)_6\text{I}_{1.70}$  iodoapatite synthesized via reactive sintering.<sup>13</sup> The 20 hr-milled sample shows an iodoapatite structure similar to that of the 10 hr-milled sample as confirmed by XRD and EDS. These results highlight a very effective approach in confining highly volatile iodine into apatite structure-type upon solid-state reaction at room temperature with greatly enhanced reaction kinetics and minimized I-volatilization by high energy ball milling.

Bridge-field TEM image (Fig. 1D) shows nano-sized particles embedded into a larger sized cluster, consistent with the SEM observation. High resolution TEM (HRTEM) images (Fig. 2a) of the 10 hr-milled sample reveal that materials exist in the form of nanocrystals embedded in a predominantly-amorphous matrix.

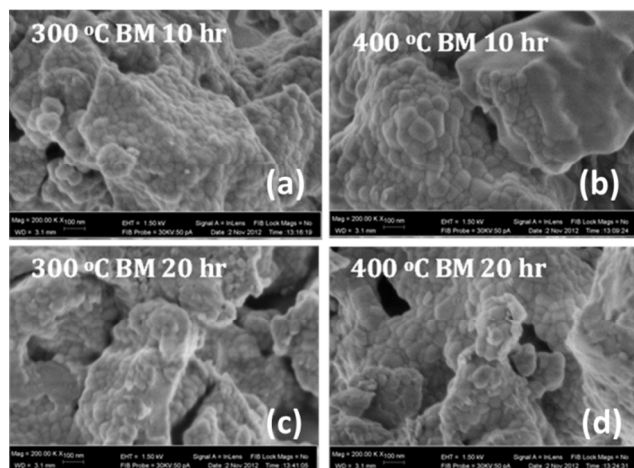


**Fig. 5** High magnification SEM images of the 20 hr ball milled sample after (a) 300 °C and (b) 400 °C thermal treatment; and the 20 hr ball milled sample after (c) 300 °C and (d) 400 °C thermal treatment.

5 This is consistent with the discrete weak diffraction spots, mostly corresponding to apatite (112), in an amorphous halo background in the selected area electron diffraction (SAED) pattern (inset in Fig. 2a). The nanocrystals are mostly 4-10 nm in size and often isolated from each other by the amorphous matrix.

10 Accompanying with the solid state reaction, the intense mechanical attrition by the high energy ball milling also caused solid-state amorphization, leading to the formation of amorphous matrix embedded with only residual nano-sized crystallites.

### 3.2 Thermally-Activated Crystallization and Phase Stability

15 As crystalline ceramic waste form may display enhanced chemical durability and thus reduced radionuclide release by incorporating and confining radionuclides into the atomic structure,<sup>16, 17</sup> crystalline iodoapatite is preferred for the confinement of iodine. Previous reports showed that thermal

20 crystallization of amorphous hydroxyapatite and fluoroapatite usually occurred at temperature higher than 600 °C.<sup>18-21</sup> However, such relatively high temperatures may be unfavorable for iodoapatite, because of phase decomposition due to iodine loss.<sup>14</sup>

25 In contrast, the as-milled iodoapatite can be well recrystallized at temperature as low as 200 °C without significant iodine loss as a result of enhanced reactivity of the powders upon mechanical attrition.

Thermal stability and recrystallization of the as-milled I-apatite were first probed by differential scanning calorimetry (DSC) at a

30 heating rate of 5 °C/min, as shown in Figure 3. A strong endothermic peak for the 10 hr milled sample was observed at 228 °C extending from ~ 190 to ~ 250 °C, corresponding to the recrystallization from almost amorphized I-apatite. The minor extended peak between 88°C and 100°C of the 20 hr milled

35 sample may be attributed to the endothermic peak of adsorbed water as a result of higher moisture adsorption due to significant grain size reduction. The calculated enthalpy of transition for the 10 hr milled sample is ~ 24.38 J/g. Similarly, the 20 hr-milled iodoapatite undergoes an exothermic process from ~ 180 to ~ 220

40 °C that peaked at 209 °C, indicating an exothermic crystallization with an enthalpy of transition of ~ 27.57 J/g. The lower exothermic peak and higher enthalpy of transition for the 20 hr milled iodoapatite can be attributed to excess free surface energy

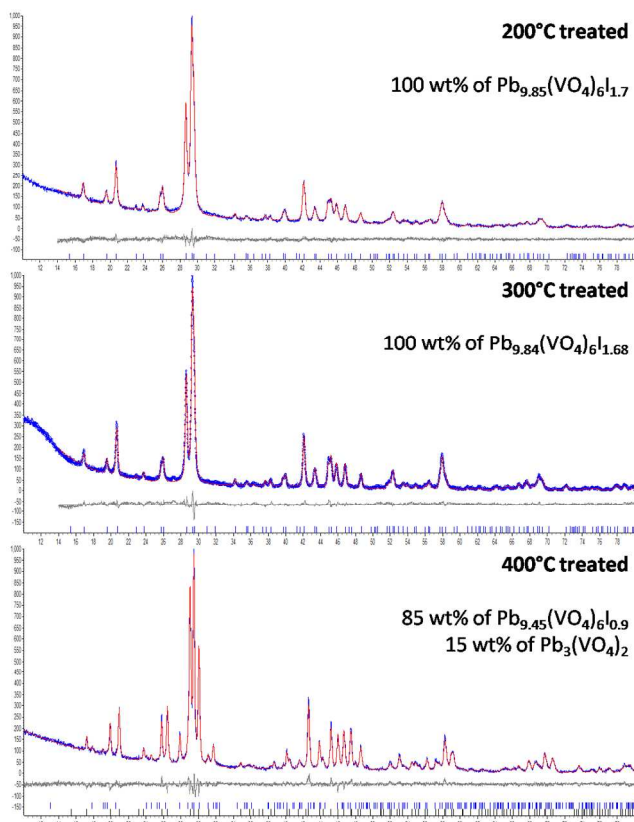


**Fig. 6** Refinement fitting of the XRD patterns of 200 °C, 300 °C and 400 °C treated iodoapatite, with blue lines representing the fit curves, red lines are the XRD patterns, gray lines are the fit to the data, and the tick marks show peak positions for the refined phases.

and possible higher defect density resulting from the longer

50 mechanical milling duration. Such an excess of free surface energy may greatly facilitate the crystallization process by reducing the energy difference between the amorphous and crystalline phases to achieve a lower transition temperature.

The as-milled iodoapatite powders were thermally treated in air at

55 temperatures of 200, 300, 400 and 550 °C for 1 hour, and the thermal stability and microstructure evolution were investigated by XRD diffraction. As shown in Figure 4, significant peak sharpening and increase in intensity of the diffraction peaks in the XRD patterns can be observed after thermal treatment at 200 °C

60 and 300 °C for both 10 and 20 hr-milled samples, indicating remarkable crystallization and grain growth due to the thermal treatment. In addition to the strongest peaks of (121), (112) and (300) at ~ 28° of two-theta, diffraction peaks corresponding to other crystal planes of lead vanadate iodoapatite also emerged

65 after 200 and 300 °C thermal treatments. Further increasing the heat treatment temperature at 400 °C, dual phases form with non-iodine bearing phase Pb<sub>3</sub>(VO<sub>4</sub>)<sub>2</sub> dominated, as a result of iodine volatilization and decomposition of iodine apatite into lead vanadate for both samples milled at 10 and 20 hrs.

70 The thermally-activated crystallization and grain growth was also observed by both *in situ* and *ex situ* TEM and SEM. *In situ* TEM was performed while heating the as-milled sample to 200 °C with a heating stage, showing that the originally amorphous matrix rapidly crystallized with grain coarsening to ~ 30 nm in only tens

75 of seconds. This is also evident by *ex situ* TEM characterization

**Table 2** Refined structural parameter of iodoapatite after 200 °C and 300 °C heat treatment.

	Atom	Site	x	y	z	Occupancy	
200 °C treated $a=10.4486\text{Å}$ $c=7.4782\text{Å}$	Pb1	4f	1/3	2/3	0.0064	0.9828	
	Pb2	12i	0.0090	0.2673	0.2743	0.4934	
	V	6h	0.3815	0.4030	1/4	1	
	O1	6h	0.4532	0.3347	1/4	1	
	O2	6h	0.4610	0.5599	1/4	1	
	O3	12i	0.2524	0.3344	0.0627	0.5	
	O4	12i	0.3239	0.4901	0.0823	0.5	
	I	12i	0.0331	0.0465	0.00047	0.1424	
	300 °C treated $a=10.4627\text{Å}$ $c=7.4773\text{Å}$	Pb1	4f	1/3	2/3	0.0066	0.9587
		Pb2	12i	0.0049	0.2665	0.2762	0.5
V		6h	0.3886	0.4048	1/4	1	
O1		6h	0.4918	0.3362	1/4	1	
O2		6h	0.4854	0.6118	1/4	1	
O3		12i	0.2299	0.3501	0.1776	0.5	
O4		12i	0.3212	0.3813	0.0497	0.5	
I		12i	0.2394	0.03233	0.0006	0.1419	

of the 300 °C treated sample which exhibits a well-crystalline grain structure with an average size of 30-50 nm (Fig. 2b). The enhanced crystallinity of the ball milled sample upon thermal treatment is also evidenced by the selected area diffraction pattern (inset in Fig. 2b). *Ex situ* SEM images show that the micron-sized granules consisting of consolidated nanoparticles are clearly observed as compared with the rough surface of the mainly amorphous, as-milled sample in Figs. 1b and 1d, the thermally-treated samples shown in Fig. 5 exhibit equant grains with well-identified grain boundaries. In addition, the larger grain size can be observed at higher annealing temperatures as a result of thermally-activated grain boundary migration and coarsening. A qualitative assessment of microstructures indicates that the thermally-treated samples, resulting from longer ball-milling times, has a finer grain size, consistent with the smaller initial particle size prior to thermal treatment. An increase of thermal treatment temperature to 400 °C leads to further grain growth. In brief, the ball milling and thermal treatment mainly affect the grain size and crystallinity of the samples. On one hand, high energy ball milling induces solid state chemical reaction to form the iodoapatite; on the other, it reduces the grain size and crystallinity of the sample via mechanical attrition. Post-milling thermal treatment below 400 °C improves the crystallinity and induces a grain growth in the sample; however, thermal treatment temperature at 400 °C or above induces significant decomposition of the iodoapatite phase.

### 3.3 Structural Characteristics of Iodoapatite by Rietveld Refinement

Rietveld refinements were performed on the XRD data revealing detailed structural characteristics of the thermally treated samples. The successful XRD data refinement of the 200, 300 and 400 °C treated samples, as indicated by the good fit of the patterns in Fig. 6, suggests that the 200 and 300 °C treated samples are a pure, iodine-bearing apatite structure. The

**Table 3** Refined key bond lengths of iodoapatite after 200 °C and 300 °C heat treatment.

200 °C treated		300 °C treated	
Bond	Length (Å)	Bond	Length (Å)
Pb1-O1	2.886	Pb1-O1	2.591
Pb1-O1	2.886	Pb1-O1	2.591
Pb1-O1	2.886	Pb1-O1	2.591
Pb1-O2	2.861	Pb1-O2	2.730
Pb1-O2	2.861	Pb1-O2	2.730
Pb1-O2	2.861	Pb1-O2	2.730
Pb1-O3	3.177	Pb1-O3	2.955
Pb1-O3	3.177	Pb1-O3	2.955
Pb1-O3	3.177	Pb1-O3	2.955
Pb2-O1	3.159	Pb2-O1	3.159
Pb2-O2	2.512	Pb2-O2	2.257
Pb2-O3	2.330	Pb2-O3	2.090
Pb2-O3	2.670	Pb2-O3	2.189
Pb2-O4	3.120	Pb2-O4	2.316
Pb2-O4	3.174	Pb2-O4	2.668
Pb2-I	2.7898	Pb2-I	3.054
Pb2-I	2.925	Pb2-I	2.985
V-O1	1.782	V-O1	1.567
V-O2	1.802	V-O2	1.877
V-O3	1.631	V-O3	1.558

structural parameters and the key bond lengths of the 200 and 300 °C treated pure iodoapatites are summarized in Tables 2 and 3. The iodoapatite samples, treated at 200 °C and 300 °C, are identical to the hexagonal apatite structure ( $P6_3/m$ ). There are two types of Pb atoms (the columnar Pb1 and axial Pb2), tightly bonded to  $\text{VO}_4$  tetrahedra and I atoms that are aligned in the channel formed by the  $\text{VO}_4$  tetrahedra corner-connected to  $\text{PbO}_6$  metaprism columns along the c-axis, as shown in Fig. 7. The  $\text{VO}_4$  unit is comprised of one V and four crystallographically nonequivalent O atoms, O1, O2, O3 and O4, with 6 sites for O1 and O2, and 12 sites for O3 and O4. The Rietveld refinement indicates that the pure iodoapatite phase in the 200 °C and 300 °C treated samples contain certain iodine and lead deficiencies, with slightly different compositions of  $\text{Pb}_{9.85}(\text{VO}_4)_6\text{I}_{1.70}$  (200 °C) and  $\text{Pb}_{9.84}(\text{VO}_4)_6\text{I}_{1.68}$  (300 °C). This iodine-deficient structure is similar to the nonstoichiometric iodoapatite  $\text{Pb}_{9.85}(\text{VO}_4)_6\text{I}_{1.70}$  reported by Audubert *et al.*<sup>13</sup> The 200 °C treated sample has a smaller lattice parameter  $a$  but a larger  $c$ -parameter than the sample treated at 300 °C. This suggests that the large iodine atom competes with the Pb for the sites in the tunnel along the  $c$ -axis. The bond lengths of V-O in the  $\text{VO}_4$  tetrahedra (Table 3) range from 1.631 to 1.802 Å for the 200 °C treated sample, and 1.567 to 1.877 Å for the 300 °C treated one, respectively. The more distorted  $\text{VO}_4$  tetrahedra in the 200 °C treated sample may be attributed to the slightly higher iodine occupancy, as inferred by the calculated chemical formula.

The two phases in the sample treated at 400 °C are evident in the XRD pattern (Figure 4) and were also determined by the Rietveld refinement as 15 wt.% of  $\text{Pb}_3(\text{VO}_4)_2$  and 85 wt.% of highly iodine-deficient  $\text{Pb}_{9.45}(\text{VO}_4)_6\text{I}_{0.9}$ , with anion vacancies along  $c$ -axis. The dominant phase of  $\text{Pb}_{9.45}(\text{VO}_4)_6\text{I}_{0.9}$  exhibits a low iodine occupancy of 0.0745 as compared with 0.1424 in the 300 °C treated sample, and the total iodine content in the double-phase sample is estimated to be ~ 1.4 at% accordingly. The highly iodine-deficient  $\text{Pb}_{9.45}(\text{VO}_4)_6\text{I}_{0.9}$  is a metastable phase that results from the partial decomposition of  $\text{Pb}_{9.84}(\text{VO}_4)_6\text{I}_{1.68}$  and can further decompose to  $\text{Pb}_3(\text{VO}_4)_2$  by release of all the iodine at higher temperatures. The complete breakdown of  $\text{Pb}_{9.45}(\text{VO}_4)_6\text{I}_{0.9}$

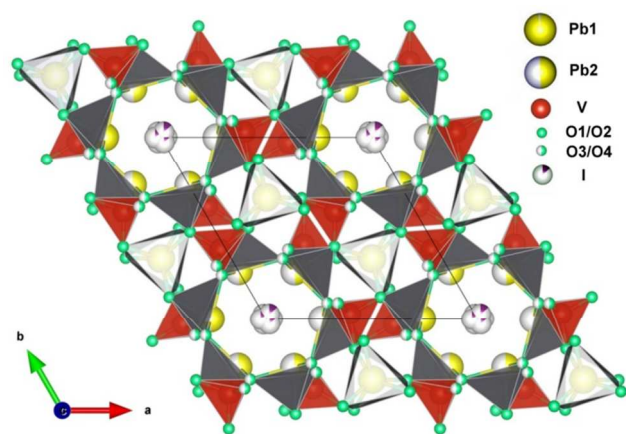


**Fig. 7** View of the  $\text{Pb}_{9.85}(\text{VO}_4)_6\text{I}_{1.7}$  crystal structure showing the I atoms in the V-O and Pb1-O polyhedral channel.

was observed when the as-milled powders were heated at 550 °C for 1 hour.

### 3.4 Micro-chemical Composition Variation upon Thermal Annealing and Iodine Confinement

Confinement of iodine is critical for the immobilization of long-lived iodine in a stable matrix because of its highly volatility. Quantitative analysis of EDX spectra of the as-milled and thermally-treated materials was performed in order to determine the correlation among microchemical composition, phase transformation, I-loss and thermal thermal annealing, in order to establish the mechanism of the phase decomposition of I-apatite at elevated temperature as a result of I-volatilization. Table I summarizes the elemental analysis of P, V, O and I for the ball-milled samples before and after thermal treatment by an EDX attached with a TEM. The iodine confinement in the synthesized powdered samples and upon thermal annealing was compared with that of ideal stoichiometric composition and iodine deficient iodoapatite determined by Rietveld refinement.

Quantitative EDS analysis indicates that iodine is well confined in the fully-crystalline iodoapatite at a low thermal annealing temperature of 200 °C and no iodine loss is observed. The iodine contents are ~4.2 at.% and 4.1 at.% for the 10 hr as-milled and 200 °C thermally-treated powders, respectively. This iodine content is consistent with the chemical formula  $\text{Pb}_{9.85}(\text{VO}_4)_6\text{I}_{1.7}$  (~4.1 at.%) as defined by the Rietveld refinement and is also similar to that previously reported by Audubert *et al.*<sup>13</sup> The iodine atomic percentage decreases slightly to ~3.6 at.% for the 300 °C thermally-treated sample, consistent with the chemical formula of  $\text{Pb}_{9.84}(\text{VO}_4)_6\text{I}_{1.68}$ . These results highlight a very effective approach of high energy ball milling in synthesizing I-bearing apatite and great iodine confinement. No significant I-loss occurs during ball milling due to the low temperature solid state reaction and post thermal annealing at a relatively-low temperature. Majority of iodine can be incorporated in the single phase apatite, which is of particular significance for the confinement of long-lived iodine.

A drastic reduction of iodine content occurs at higher annealing temperatures with a reduction of iodine level from ~3.6 at.% in the 300 °C treated sample to ~1.1 at.% after the 400 °C thermal treatment. Such a reduced iodine content at 400 °C indicates the

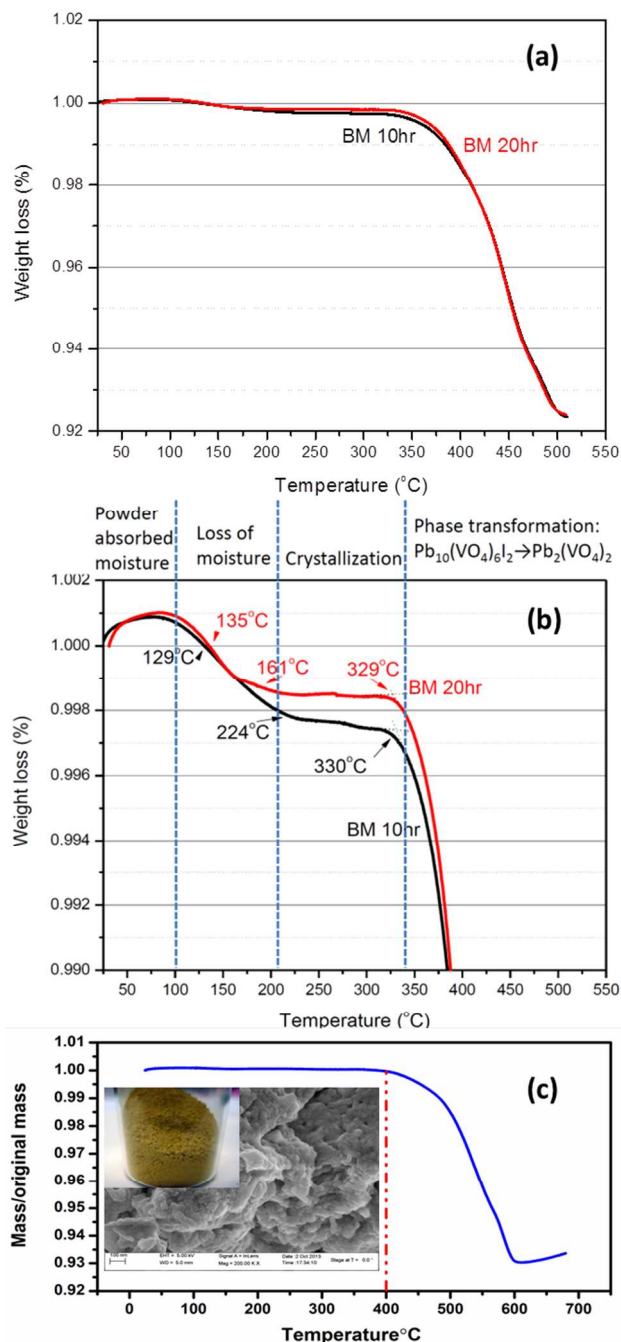


**Fig. 8** TGA curves of ball-milled samples: (a) as-milled iodoapatite samples, with the black line showing the 10 hr milled sample and the red line showing the 20 hr milled sample; (b) a close-up of the TGA curves of (a); and (c) crystalline iodoapatite powders upon 10 hr ball milling and thermal treated at 200 °C for 1 hr. Significant enhancement in the thermal stability and phase decomposition temperature are identified. A high iodine loading (~7 wt%) was observed in the thermally annealed samples.

loss of iodine due to the decomposition of the iodoapatite structure to lead vanadate  $\text{Pb}_3(\text{VO}_4)_2$ , consistent with the XRD data. The decomposition of iodoapatite observed at 400 °C releases the highly volatile free iodine, of which the low boiling point of iodine (184.3 °C) and strong tendency of sublimation can lead to  $\text{I}_2$  gas release.

TGA was utilized to investigate the decomposition and iodine loss of the iodoapatite at elevated temperatures. The TGA curves

in Fig. 8a showed the weight changes of the 10 h and 20 milled powder samples in a temperature range from 25 to 510 °C. Both samples were generally stable up to ~ 330 °C in air with no significant weight change. A close-up TGA spectrum is shown in Fig. 8b, in which different stages of crystallization and phase decomposition can be clearly identified. Particularly, the onset of weight loss began at ~ 330 °C, followed by a steep edge at ~ 380 °C that extend and saturate afterward to 500 °C. The total loss of weight was ~ 7.6 wt% for both samples, close to the weight percentage of iodine (~ 7.3 wt%) in the  $\text{Pb}_{9.85}(\text{VO}_4)_6\text{I}_{1.70}$  and  $\text{Pb}_{9.84}(\text{VO}_4)_6\text{I}_{1.68}$  iodoapatite structures. Therefore, we conclude that the decomposition and iodine loss for the HEBM synthesized iodoapatite occur mainly between 330 and 500 °C, and the phase decomposition and the release of gaseous  $\text{I}_2$  accounts for most of the weight loss.

The subsequent annealing process at a low temperature 200 °C greatly improves the thermal stability and increases the phase decomposition temperature due to the high crystalline feature and noticeable grain coarsening. The on-set temperature for iodine loss increases to 400 °C and no significant weight loss (only ~1 wt.%) was observed above 500 °C for the loosely-packed powders (as shown in Figure 8c) upon 200 °C thermally treatment. Complete iodine loss (~7 wt%) occurs at the temperature above 600 °C. As compared with Fig. 8a, no moisture absorption is found in Fig. 8c because the significant grain growth upon thermal annealing dramatically reduced the specific surface area of the iodoapatite sample and hence the moisture absorption.

### 3.5 Impact and Significance of HEBM Process for Iodine Immobilization

The HEBM synthesis of high-iodine iodoapatite demonstrated in this study features a facile one-step solid state reaction at low temperature (~ 50 °C) with a high iodine loading. The as-milled sample in the form of amorphous-dominated matrix can readily be crystallized at temperatures as low as 200 °C without any iodine loss. This simple and efficient synthesis approach allows large scale processing iodine-bearing waste forms for the immobilization of long lived fission product I-129.

The low temperature solid state reaction by HEBM and subsequent low temperature annealing offer distinct advantages for developing durable waste forms for effective confinement of volatile radionuclides. Previous methods, e.g., 500-700 °C for conventional hot pressing and ~ 500 °C for microwave heating,<sup>1,3,12,15</sup> inevitably require heating the samples to relatively high temperatures, leading to significant phase decomposition and iodine release.<sup>14</sup> In such cases, the chemical processing system must be confined, such as with sealed containers or embedding the reactants in an orthovanado-phosphate matrix.<sup>1, 3, 15</sup> In contrast, high-loading of iodine can be achieved for the single phase iodoapatite by the facile, low-temperature approach by HEBM.

It is worth noting that the our HEBM synthesized iodoapatite exhibits improved thermal stability as compared with the previously reported high temperature sintered iodoapatite, which begins to decompose to lead ortho-vanadate  $\text{Pb}_3(\text{VO}_4)_2$  at only 270 °C and completely loses its iodine at above 407 °C.<sup>14</sup> Although a higher mass loss temperature of 500 °C was reported for the iodoapatite prepared by microwave dielectric heating, it is

noted that dense iodoapatite pellets with 10% of  $\text{Pb}_3(\text{VO}_4)_2$  buffer phase was used for TGA testing in that study,<sup>12</sup> rather than the loosely packed nano-sized powders as the current work. The thermal stability improvement for HEBM synthesized iodoapatite may be due to the low reaction temperature (~ 50 °C) during the ball milling process as compared with the 500-700 °C temperature for the various heating techniques as previously reported.<sup>3, 12</sup> At such a low temperature, thermal decomposition and destabilization of the iodoapatite can be greatly mitigated, resulting in enhanced thermal stability of the powdered samples with a complete iodine loss above 500 °C. In addition, the subsequent annealing process at low temperature 200 °C will further improve the thermal stability due to the high crystalline feature and noticeable grain coarsening. No significant weight loss (only ~1 wt.%) was observed above 500 °C for the loosely-packed powders (as shown in Figure 8c) upon 200 °C thermally treatment and complete iodine loss occurs at 600 °C.

For consolidation of iodoapatite into durable waste forms, very rapid heating techniques such as spark plasma sintering (SPS) and microwave heating<sup>11, 12</sup> will be particularly useful in order to minimize iodine release associated with the densification. The nano-scale features and surface activation upon mechanical attrition of HEBM will greatly improve the sinterability and reactivity of the ball-milled powders, beneficial for the densification and consolidation process. The improved sinterability and reactivity of the ball milled samples were already demonstrated by the enhanced kinetics for rapid recrystallization and grain growth at temperature (200 °C), far below the decomposition temperature of iodoapatite. Using ball-milled powders and spark plasma sintering, we have fabricated fully dense iodoapatite ceramic pellets at temperatures of 700 °C within a very short duration (e.g., several minutes) with greatly-improved thermal stability and iodine confinement, as compared with previously-fabricated iodoapatite pellets by SPS or microwaving sintering.<sup>11,12</sup> The study on rapid consolidation of iodoapatite will be reported elsewhere.<sup>22</sup>

## 4. Conclusions

In summary, we report a novel low temperature solid-state approach of synthesizing iodine-bearing apatite by high-energy ball milling combining with low temperature post thermal annealing. In contrast to previously reported synthesis methods which required heating at elevated temperature, the HEBM approach is a facile and one-step solid reaction at low temperature driven by mechanical attrition such that the iodine loss occurring at elevated temperatures can be greatly mitigated. The as-milled samples exist in the form of nanocrystals embedded in an amorphous matrix, and the crystals can be readily recrystallized into a pure, single-phase iodoapatite at 200 °C. As compared to iodoapatite obtained by conventional methods, the ball-milled iodoapatite has a lower crystallization temperature, improved thermal stability, a higher decomposition temperature and excellent iodine confinement. The successful development of this new approach opens up the opportunity for synthesizing a wide range of different iodine-bearing apatite compositions as stable waste forms for the immobilization and safe disposal of long-lived, radiotoxic fission product I-129.

## Acknowledgements

This work is supported by DOE NEUP (Nuclear Engineering University Program) under the award DE-AC07-05ID14517 and a NSF career award DMR 1151028. ZL Dong acknowledges the support from a Singapore NTU AcRF grant RG11/04.

<sup>a</sup> Department of Mechanical, Aerospace, and Nuclear Engineering, Rensselaer Polytechnic Institute, Troy, NY 12180, USA; E-mail: lianj@rpi.edu

<sup>b</sup> School of Materials Science and Engineering, Nanyang Technological University, Singapore 639798

<sup>c</sup> Department of Geological & Environmental Sciences, Stanford University, Stanford, CA 94305-2115

## Notes and references

- 1 C. Guy, F. Audubert, J. E. Lartigue, C. Latrille, T. Advocat and C. Fillet, *C. R. Phys.*, 2002, **3**, 827.
- 2 N. C. Hyatt, J. A. Hriljac, A. Choudhry, L. Malpass, G. P. Sheppard and E. R. Maddrell, *Mater. Res. Soc. Symp. Proc.*, 2004, **807**, 359.
- 3 F. Audubert, J. Carpena, J. L. Lacout and F. Tetard, *Solid State Ionics*, 1997, **95**, 113.
- 4 G. Lefevre, J. Bessiere, J. J. Ehrhardt and A. Walcarius, *J. Environ. Radioact.*, 2003, **70**, 73.
- 5 S. Wu, S. Wang, A. Simonetti, F. Chen and T. E. Albrecht-Schmitt, *Radiochim. Acta*, 2011, **99**, 573.
- 6 F. Y. Lu, Z. L. Dong, J. M. Zhang, T. White, R. C. Ewing and J. Lian, *RSC Adv.*, 2013, **3**, 15178.
- 7 Z. L. Dong, T. J. White, B. Wei and K. Laursen, *J. Am. Ceram. Soc.*, 2002, **85**, 2515.
- 8 T. J. White and Z. L. Dong, *Acta Crystallogr., Sect. B: Struct. Sci.*, 2003, **59**, 1.
- 9 J. L. Fleche, *Phys. Rev. B*, 2002, **65**, 245116.
- 10 L. Merker and H. Wondratschek, *Z. Anorg. Allg. Chem.*, 1959, **300**, 41.
- 11 S. Le Gallet, L. Campayo, E. Courtois, S. Hoffmann, Y. Grin, F. Bernard, and F. Bart, *J. Nucl. Mater.*, 2010, **400**, 251.
- 12 M. C. Stennett, I. J. Pinnock and N. C. Hyatt, *J. Nucl. Mater.*, 2011, **414**, 352.
- 13 F. Audubert, J. M. Savariault and J. L. Lacout, *Acta Crystallogr., Sect. C: Cryst. Struct. Commun.*, 1999, **55**, 271.
- 14 S. A. T. Redfern, S. E. Smith and E. R. Maddrell, *Mineral. Mag.*, 2012, **76**, 997.
- 15 M. Uno, M. Shinohara, K. Kurosaki and S. Yamanaka, *J. Nucl. Mater.*, 2001, **294**, 119.
- 16 R. C. Ewing, W. J. Weber and W. Lutze, *Disposal of Weapon Plutonium 1996*, **4**, 65.
- 17 G. R. Lumpkin, *Elements*, 2006, **2**, 365.
- 18 I. Cacciotti, A. Bianco, M. Lombardi and L. Montanaro, *J. Eur. Ceram. Soc.*, 2009, **29**, 2969.
- 19 K. A. Gross, V. Gross and C. C. Berndt, *J. Am. Ceram. Soc.*, 1998, **81**, 106.
- 20 M. Hidouri, K. Bouzouita, F. Kooli, and I. Khattech, *Mater. Chem. Phys.*, 2003, **80**, 496.
- 21 P. Layrolle, A. Ito and T. Tateishi, *J. Am. Ceram. Soc.*, 1998, **81**, 1421.
- 22 T. K. Yao, F. Lu, H. T. Sun, J. W. Wang, R. C. Ewing and J. Lian, *J. Am. Ceram. Soc.*, in press (doi: 10.1111/jace.13101).